Local atomic structures for tunable ordered arrangements of crystallographic shear planes in titanium-chromium oxide natural superlattices

Shunta Harada,[1,2,3†] Shunya Sugimoto,[2†] Naoki Kosaka,[2] Miho Tagawa,[1,2] Toru Ujihara[1,2,4]*

[1] *Center for Integrated Research of Future Electronics (CIRFE), Institute of Materials and Systems for Sustainability (IMaSS), Nagoya University, Furo-cho, Chikusa-ku, Nagoya 464-8601, Japan*

[2] *Department of Materials Process Engineering, Nagoya University, Chikusa-ku, Furo-cho, 464-8603, Nagoya, Japan*

[3] *PRESTO, Japan Science and Technology Agency, 4-1-8 Honcho, Kawaguchi-shi, Saitama 332-0012, Japan*

[4] *GaN Advanced Device Open Innovation Laboratory (GaN-OIL), National Institute of Advanced Industrial Science and Technology (AIST), Nagoya University, Furo-cho, Chikusa-ku, Nagoya 464-8601, Japan*

[†]*Authors equally contributed to this paper.*

Keywords

natural superlattice, crystallographic shear structure, incommensurate structures,

specularity parameter

Abstract

The atomic structure of titanium-chromium oxide natural superlattices with different compositions having an ordered arrangement of crystallographic shear (CS) planes was investigated by high-angle annular dark-field (HAADF) scanning transmission electron microscopy (STEM) as well as electron diffraction, using polycrystalline ceramics prepared by arc-melting and heat treatment. Analysis of the electron diffraction patterns revealed that not only the interspacing but also the direction of planar faults changed depending on the chromium concentration. HAADF-STEM observations showed that the atomic arrangements of CS planes deviating from $(121)_{rutile}$ are random arrangements of $(121)_{rutile}$ CS planes and $(011)_{rutile}$ anti-phase boundaries. Using a random walk model as well as by calculating the specularity parameter, we found that the CS planes in titanium-chromium oxides behave as coherent interfaces for phonons based on the estimation of interface roughness.

Introduction

Coherent manipulation and control of heat by nanoscale periodic structures, which is different from the diffuse picture of thermal transport[1–6], has attracted great attention owing to the potential for advanced thermal management. Coherent thermal transport has

been investigated using phononic crystals, artificial superlattice thin films and nanostructured materials[7–11]. Phononic crystals, which are fabricated by advanced lithography techniques, can be designed with dimensions of more than a hundred nanometers with a high degree of freedom, and demonstrate control of low frequency phonons (on the order of up to hundreds of gigahertz) and thermal transport at low temperature (less than 10 K)[3,12–14]. Artificial superlattice thin films grown by chemical vapor deposition, molecular beam epitaxy and sputtering methods are suitable systems for the investigation of coherent heat conduction in nanoscale periodic structures[15,16]. Some researchers have reported the observation of coherent heat conduction in superlattices[17–19]. Ravichandran et al. demonstrated the crossover from incoherent to coherent phonon scattering from the results of thermal conductivity measurements of high-quality perovskite superlattices of $SrTiO_3/CaTiO_3$ and $SrTiO_3/BaTiO_3$ with different periods. However, the interfaces in superlattices are inevitably too rough for thermal phonons of terahertz order to be diffusely scattered and tend to behave incoherently.[16,20–24]. In our previous study, we reported that periodically introduced planar faults in titanium oxide natural superlattices with crystallographic shear (CS) structures have high structural perfection, and the interface roughness for the planar faults in these natural superlattices was estimated to be one order magnitude smaller than that obtained for the interfaces of artificial superlattices, and coherent heat conduction in this system was expected[25].

The other important feature of this natural superlattice system is that the spacings of the periodically introduced planar faults can be tuned by composition. In homologous series of binary titanium oxides expressed by Ti_nO_{2n-1} (n = 4, 5, …), dense planar faults called CS planes are regularly introduced with their spacing depending on the oxygen

deficiency[26,27]. Here, we focused on another homologous series of titanium-chromium oxides and related phases with CS structures because titanium-chromium oxides are electrically insulating and it is possible to directly derive coherent heat conduction from measurements of thermal conductivity without considering electrical contributions to the thermal conductivity[28].In the present study, we investigated the local atomic structures of CS planes in titanium-chromium oxides.

Crystal structures of titanium-chromium oxides

Crystallographic shear structures in titanium oxides, which were first confirmed in the 1950s and have since been intensively studied by several researchers[27,29–37], contain an ordered arrangement of CS planes, on which the atomic arrangement deviates from the mother lattice by a certain vector called the CS vector. Titanium-chromium oxides with CS structures were first reported by Andersson et al.[30], and have been investigated from the viewpoint of their structure and phase relationships[34–38]. Somiya et al. carefully examined the phase relationships of Cr_2O_3-TiO_2 as well as the crystal structure by analysis of X-ray diffraction (XRD) and electron diffraction patterns, and came to the following conclusions related to phases with CS structures having rutile as the mother structure[38]:

(1) The homologous series of titanium-chromium oxides expressed as $Cr_2Ti_{n-2}O_{2n-1}$ with n = 6, 7, 8 are stable as single phases with $(121)_{rutile}$ CS structures in certain temperatures ranges.

(2) Continuously ordered solid solution (COSS) phases with CS structures in which the CS planes continuously rotate from $(121)_{rutile}$ to $(132)_{rutile}$, with spacing changes dependent on the composition, are stable below 1425°C in the composition range of

14 to 22 wt% Cr_2O_3.

(3) The solubility limit of rutile is 7 wt% Cr_2O_3.

The $(hkl)_{rutile}$ CS planes for the COSS phase, which lie on the $[1\text{-}11]_{rutile}$ zone axis, can be generally described as follows[35];

$$(hkl)_{rutile} = p(121)_{rutile} + q(011)_{rutile}$$
$$= (p, 2p+q, p+q)_{rutile}$$
$$= (p+q)(p', 1+p', 1)_{rutile}, \qquad (1)$$

where p and q are integers and p' is $p/(p+q)$. The last term is a pseudo-Miller index $(h'k'l')_{rutile}$ since p' is not an integer. Here, we define the spacing of the $(h'k'l')_{rutile}$ plane as

$$d_{h'k'l'} = (p + q)d_{hkl} \qquad (2)$$

where d_{hkl} stands for the interplanar distance of $(hkl)_{rutile}$. The $(121)_{rutile}$ and $(132)_{rutile}$ CS planes are special cases of the general formula expressed as Eq. (1), in which the set of values (p, q) = (1, 0) and (1, 1) (the value p' = 1 and 0.5), respectively. The stacking sequence of the $(hkl)_{rutile}$ planes can be expressed as -**BAB BAB BAB**-, where **A** denotes a titanium layer (**A** = Ti) and **B** denotes an oxygen layer (**B** = O). The presence of the CS plane (denoted as *) changes the sequence to -**BAB BA*BAB**-. If the CS plane is introduced every n titanium layers (**A**), the composition is described as $Cr_{2p}Ti_{n-2p}O_{2n-p}$ and $Cr_{2p'}Ti_{n'-2p'}O_{2n'-p'}$ where n' is $n/(p+q)$. The ideal CS vector has a collapse component normal to $(hkl)_{rutile}$ and the ideal spacing of the CS plane (D_{CS}) is described as follows:

$$D_{CS} = d_{hkl}(n - p/2)$$
$$= d_{h'k'l'}(n' - p'/2). \qquad (3)$$

When the CS planes are introduced in the mother rutile structure, lines of superlattice reflection spots along the reciprocal lattice vector corresponding to the CS

plane appear at the positions corresponding to n. The electron diffraction pattern expected for the COSS phase with the $(374)_{rutile}$ CS plane (p = 3, q = 1, p' = 0.75) and n = 44 as well as the corresponding structure of $Cr_6Ti_{38}O_{85}$ are depicted in Fig. 1. Note that a line of superlattice reflection spots along $\boldsymbol{g}(374)_{rutile}$ internally divides the line connecting $\boldsymbol{g}(121)_{rutile}$ and $\boldsymbol{g}(132)_{rutile}$ at $(1 - p')$: p'. Furthermore, the spacing of the CS planes can be evaluated from the interval of the superlattice reflection spots s:

$$D_{CS} = L\lambda/s, \qquad (4)$$

where L and λ stand for the camera length and wavelength of electron beam. Namely, the orientation and spacing of the CS planes can be estimated from the electron diffraction patterns. Note that the set of values for p and q is not necessarily integer. Therefore, the COSS phase is a kind of incommensurate phase except for the special cases with the set of values for p and q is integer.

Although the direction and interspacing of the CS planes were thoroughly investigated by electron diffraction as well as high-resolution TEM[34,36,37,39], the local atomic structure of a CS plane which deviates from the $(121)_{rutile}$ plane has never been reported so far. Especially, in CS planes deviating from $(121)_{rutile}$, which is not represented by the Miller index with integers, it is expected that a kind of randomness is inevitably introduced in the atomic arrangements. Although we have already reported that the picoscale structural perfection of the commensurate $(132)_{rutile}$ CS structure, the local atomic structures as well as the structural perfection of the incommensurate CS structure has not clarified yet. Not only from the viewpoint of phonon coherence but also from the

viewpoint of crystallography, the local atomic structure in the CS planes is worth attracting interest. Therefore, in the present study, we intensively investigated the atomic arrangement of titanium oxides with a CS structure by high-angle annular dark-field scanning transmission electron microscopy (HAADF-STEM) imaging combined with electron diffraction.

Experimental

High-purity TiO_2 and Cr_2O_3 powders weighed in appropriate ratios were mixed and pressed into pellets. Then, the pellets of mixed powders were sintered at 1423 K for 24 h in air. Polycrystals were prepared from the sintered pellets by arc-melting in an Ar gas atmosphere. The polycrystals were annealed at 1673 K in air. Nominal compositions of the prepared specimens are tabulated in Table I.

Powder specimens for XRD and TEM analysis were prepared by grinding the polycrystals in a zirconia mortar. Phase identification was carried out by powder XRD using a RINT-2500TTR diffractometer (Rigaku Co. Ltd.). The crystal structures were investigated by TEM and HAADF-STEM using JEM-2010F and JEM-ARM200 (JEOL Co. Ltd.) transmission electron microscopes. Drops of dispersions of the powder specimens were deposited on a carbon-coated copper grid (Okenshoji Co. Ltd., elastic carbon coated Cu mesh), left to dry under vacuum and then (S)TEM observations were performed at 200 kV.

Results

Figure 2 shows XRD patterns for the prepared specimens of TiO_2 and TiO_2-24.1 wt% Cr_2O_3 with different annealing conditions. The XRD pattern from as-arc-melted TiO_2 without annealing exhibits many weak peaks in addition to the peaks from the rutile structure. This indicates that the structure of the as-arc-melted specimen was a rutile-based superstructure, such as a CS structure, due to the occurrence of oxygen deficiency during arc-melting in an inert gas. After annealing at 1673 K for 24 h in air, all the weak peaks other than those from the rutile structure were eliminated, indicating that this annealing condition is sufficient to oxidize the specimen. On the other hand, in the XRD pattern from the TiO_2-24.1 wt% Cr_2O_3 specimen annealed at 1673 K for 24 h, peaks were observed not only from $Cr_2Ti_6O_{15}$ but also other peaks from a homologous series of $Cr_2Ti_{n-2}O_{2n-1}$ and E phase ($Cr_2Ti_2O_7$)[39,40], and other unknown peaks similar to those from the CS structure, indicating that the specimen were not in thermal equilibrium under this annealing condition. The specimen reached thermal equilibrium after increasing the annealing time, and finally the XRD peaks from the specimen annealed for 100 h were almost all consistent with those from $Cr_2Ti_6O_{15}$ reported by Kamiya et al[39]. Figure 3 shows XRD patterns of annealed specimens prepared with different nominal compositions. The phases identified for each of the specimens are summarized in Table I. While essentially only a single phase was identified for the specimen of TiO_2-24.1 wt% Cr_2O_3 as expected from the nominal composition, the specimen of TiO_2-27.6 wt% Cr_2O_3 contained $Cr_2Ti_5O_{13}$ as a major phase with a minor inclusion of $Cr_2Ti_6O_{13}$. Considering that the nominal composition of TiO_2-27.6 wt% Cr_2O_3 is expected to form $Cr_2Ti_6O_{13}$, the composition underwent a slight change due to evaporation of Cr_2O_3 during arc-melting and annealing at high temperature. The other specimens with TiO_2-15.0 and 20.0 wt%

Cr_2O_3 exhibited similar XRD patterns to those from the homologous series of $Cr_2Ti_{n-2}O_{2n-1}$ with slight differences in diffraction angles, implying that CS structures of COSS phases formed in the specimens.

Figure 4 shows selected area electron diffraction (SAED) patterns taken along the $[1\text{-}11]_{rutile}$ zone axis for the prepared specimens after annealing at 1673 K for 24 h. Lines of superlattice reflection spots indicating the introduction of ordered arrangements of the CS planes were observed for all titanium-chromium oxides. In the SAED pattern taken from the specimen of TiO_2-27.6 wt% Cr_2O_3 shown in Fig. 4(d), the superlattice spots are indeed directed along $(121)_{rutile}$ and the interval of the superlattice spots corresponds to 7 times the interspacing of $(121)_{rutile}$, in agreement with the $(121)_{rutile}$ CS structure of $Cr_2Ti_5O_{13}$, which was identified in this specimen by powder XRD. In the SAED pattern taken from the specimen of TiO_2-24.1 wt% Cr_2O_3 shown in Fig. 4(c), the superlattice spots are directed almost along $(121)_{rutile}$ and located at the positions that divide $\boldsymbol{g}(121)_{rutile}$ into 8 approximately equal intervals. This indicates that the structure and the composition of the specimen deviate slightly from $Cr_2Ti_6O_{15}$ with the $(121)_{rutile}$ CS structure to a COSS phase. The SAED patterns from the specimens of TiO_2-15.0 and 20.0 wt% Cr_2O_3 shown in Figs. 4(a) and 4(b) exhibit the occurrence of an ordered arrangement of CS planes slightly tilted from $(121)_{rutile}$ to $(132)_{rutile}$, indicating that the specimens are composed of COSS phases. Table II summarizes the values of p' and D_{CS} estimated from the SAED patterns. The interspacing and the deviation from the $(121)_{rutile}$ of the CS planes increases with decreasing Cr_2O_3 concentration.

Figure 5 shows HAADF-STEM images taken along the $[1\text{-}11]_{rutile}$ zone axis from the prepared specimens after annealing. In the HAADF-STEM images, Ti/Cr atom

columns are imaged as bright spots, while O atom columns are not imaged. The arrangements of Ti/Cr atom columns deviate on the CS planes. The intervals of the CS planes increase with decreasing Cr_2O_3 concentration. Figure 6 shows magnified HAADF-STEM images taken from the prepared specimens. No imperfection in the atomic arrangement for the $(121)_{rutile}$ CS planes in $Cr_2Ti_5O_{13}$ phase with a nominal composition of TiO_2-27.6wt%Cr_2O_3 was noticed by HAADF-STEM observation. As observed in the SAED patterns shown in Fig. 4, the CS planes in the crystals with nominal compositions of TiO_2-15.0, 20.0 wt% and 24.1wt% Cr_2O_3 deviate from the $(121)_{rutile}$ plane and contain randomly alternating $(121)_{rutile}$ CS planes and $(011)_{rutile}$ antiphase boundaries (APBs). Each APB corresponds to a one-layer deviation of the $(121)_{rutile}$ CS planes. At some positions in the CS plane, multiple APBs were successively located, as shown in Fig. 5(a).

Discussion

Assuming the Debye model, the mean free path for phonons (l) can be evaluated from the following equation and reported values[41,42],

$$\kappa = \frac{1}{3} C_p \rho v l, \qquad (5)$$

where κ, C_p, ρ, and v stand respectively for the thermal conductivity, specific heat, density, and sound velocity. The mean free path for phonons in a rutile TiO_2 single crystal along the [100] direction is evaluated to be 2.0 nm at room temperature from the reported values of specific heat, thermal conductivity, density and sound velocity, which is comparable to the interspacing of the CS planes (1.1~1.9 nm) observed in polycrystals of titanium-chromium oxide superlattices, and coherent thermal transport is expected to become

apparent in the thermal conduction in titanium-chromium oxide natural superlattice single crystals with an ordered arrangement of CS planes, if the mean free path of the mother rutile structure in the CS structures of titanium-chromium oxides is assumed to be similar to the rutile TiO_2.

As can be seen in the SAED patterns shown in Fig. 4, the superlattice reflection spots were sharp and the CS planes in titanium-chromium oxides were perfectly arranged. However, HAADF-STEM observations revealed that the atomic arrangement of the CS planes deviating from $(121)_{rutile}$ is a random arrangement of $(121)_{rutile}$ CS planes and $(011)_{rutile}$ APBs. If we assume that the arrangement is completely random (here referred to as the "random walk model"), the expected value of the root mean square (RMS) roughness R_{RWM} for CS planes expressed with the pseudo Miller index of $p'(121)_{rutile} + q'(011)_{rutile}$ ($p' + q' = 1$) is calculated from the one-dimensional random walk model:

$$R_{RWM} = p'(1 - p')d', \quad (6)$$

where d' is the interspacing of the pseudo Miller index defined by Eq. (2). From the SAED patterns, one can obtain the values of p' and estimate the interface roughness from Eq. (6). Estimated values of the RMS roughness and the interspacing for the CS planes depending on chromium content are plotted in Fig. 7. As the concentration of Cr_2O_3 decreases, the RMS roughness increases, resulting from increasing deviation of the CS planes from $(121)_{rutile}$. Here, we discuss the influence of the geometrical arrangement of the CS planes on the interface roughness by calculating the specularity parameter (p_s). The specularity parameter, which describes whether the interface coherently scatters an incident phonon ($p_s = 1$) or not ($p_s = 0$), is expressed as follows depending on the frequency (f);[43]

$$p_s(f) = exp(-16\pi^2(\frac{Rf}{v})^2), \qquad (7)$$

where R and v stand for the RMS roughness of the interface and the group velocity of phonons, respectively. Wagner et al. suggested that $p_s > 0.3$ constitutes a criterion for a coherent interface for phonons[13]. Following the criterion, it is expected that the CS planes, even in the specimen with the nominal composition of TiO_2-15.0wt%Cr_2O_3, which has the largest RMS roughness among the prepared specimens as estimated by the random walk model, behave as coherent interfaces for phonons with a frequency less than 15.2 THz. Considering that the highest phonon mode frequency (top of the optical mode) in rutile TiO_2 was reported to be around 25 THz[44], the rotation of the CS planes in COSS phases has little influence on the coherence of most thermal phonons.

Although CS planes would have imperfections that were not noticed by the HAADF-STEM observations, these planes are considered to have sufficient structural perfection to behave as coherent interfaces for thermal phonons, and the deviation of the CS planes from $(121)_{rutile}$ would have little influence on the coherence of the interfaces. Titanium-chromium oxide natural superlattices with an ordered arrangement of CS planes, of which the interspacing can be tuned by modulation of the Cr_2O_3 concentration, represent a suitable system for the investigation of coherent heat conduction in nanoscale periodic structures.

Conclusion

The atomic structure of titanium-chromium oxide natural superlattices with an ordered arrangement of CS planes with different compositions was investigated using

polycrystalline ceramics prepared by arc-melting and heat treatment. The results obtained are summarized as follows:

(1) The polycrystalline ceramics were reduced during arc-melting in an argon atmosphere, and subsequent heat treatment in air at 1673 K oxidized the ceramics.

(2) By changing the Cr_2O_3 concentration, the interspacing of the CS planes can be tuned over the range 1.1 to 1.9 nm accommodating the rotation of the CS planes.

(3) The atomic arrangement of the $(121)_{rutile}$ CS planes in the $Cr_2Ti_5O_{13}$ phase was almost perfect and no imperfections were detected by HAADF-STEM observations.

(4) The structures of the CS planes deviating from $(121)_{rutile}$ in COSS phases were composed of an alternating disordered arrangement of $(121)_{rutile}$ CS planes and $(011)_{rutile}$ APBs.

(5) From the estimation of the RMS roughness by a random walk model as well as calculation of the specularity parameter for the CS planes, the deviation of the CS planes from $(121)_{rutile}$ should have little influence on the coherence of the interface.

AUTHOR INFORMATION

Corresponding Author

* Shunta Harada

Institute of Materials and Systems for Sustainability, Nagoya University, Furo-cho, Chikusa-ku, Nagoya, 464-8601 Japan; E-mail: shunta.harada@nagoya-u.jp

Author Contributions

S. H. conceived and designed the experiments and the analysis. S. S. and S. H. carried out the experiments and the analysis with N. K. The experimental data and analysis were discussed by all authors. The manuscript was written by S. H. in discussion with all the authors. All authors have given approval for the final version of the manuscript.

Note

The authors declare no competing financial interest.

ACKNOWLEDGMENT

This work was partly supported by JST PRESTO (JPMJPR18I8) and Grant-in-Aid for Scientific Research (B) from MEXT (18H01733).

REFERENCES

(1) Narayanamurti, V. Phonon Optics and Phonon Propagation in Semiconductors. *Science.* **1981**, *213* (4509), 717–723.

(2) Simkin, M. V.; Mahan, G. D. Minimum Thermal Conductivity of Superlattices. *Phys. Rev. Lett.* **2000**, *84* (5), 927–930.

(3) Yu, J. K.; Mitrovic, S.; Tham, D.; Varghese, J.; Heath, J. R. Reduction of Thermal Conductivity in Phononic Nanomesh Structures. *Nat. Nanotechnol.* **2010**, *5* (10), 718–721.

(4) Dechaumphai, E.; Chen, R. Thermal Transport in Phononic Crystals: The Role of Zone Folding Effect. *J. Appl. Phys.* **2012**, *111* (7).

(5) Maldovan, M. Sound and Heat Revolutions in Phononics. *Nature* **2013**, *503* (7475), 209–217.

(6) Maldovan, M. Phonon Wave Interference and Thermal Bandgap Materials. *Nat. Mater.* **2015**, *14* (7), 667–674.

(7) Wingert, M. C.; Chen, Z. C. Y.; Dechaumphai, E.; Moon, J.; Kim, J. H.; Xiang, J.; Chen, R. Thermal Conductivity of Ge and Ge-Si Core-Shell Nanowires in the Phonon Confinement Regime. *Nano Lett.* **2011**, *11* (12), 5507–5513.

(8) Chen, J.; Zhang, G.; Li, B. Impacts of Atomistic Coating on Thermal Conductivity of Germanium Nanowires. *Nano Lett.* **2012**, *12* (6), 2826–

2832.

(9) Luckyanova, M. N.; Mendoza, J.; Lu, H.; Song, B.; Huang, S.; Zhou, J.; Li, M.; Dong, Y.; Zhou, H.; Garlow, J.; et al. Phonon Localization in Heat Conduction. *Sci. Adv.* **2018**, *4* (12), eaat9460.

(10) Uematsu, Y.; Terada, T.; Sato, K.; Ishibe, T.; Nakamura, Y. Low Thermal Conductivity in Single Crystalline Epitaxial Germanane Films. *Appl. Phys. Express* **2020**, *13* (5), 055503.

(11) Taniguchi, T.; Terada, T.; Komatsubara, Y.; Ishibe, T.; Konoike, K.; Sanada, A.; Naruse, N.; Mera, Y.; Nakamura, Y. Phonon Transport in the Nano-System of Si and SiGe Films with Ge Nanodots and Approach to Ultralow Thermal Conductivity. *Nanoscale* **2021**, *13* (9), 4971–4977.

(12) Alaie, S.; Goettler, D. F.; Su, M.; Leseman, Z. C.; Reinke, C. M.; El-Kady, I. Thermal Transport in Phononic Crystals and the Observation of Coherent Phonon Scattering at Room Temperature. *Nat. Commun.* **2015**, *6*.

(13) Wagner, M. R.; Graczykowski, B.; Reparaz, J. S.; El Sachat, A.; Sledzinska, M.; Alzina, F.; Sotomayor Torres, C. M. Two-Dimensional

Phononic Crystals: Disorder Matters. *Nano Lett.* **2016**, *16* (9), 5661–5668.

(14) Maire, J.; Anufriev, R.; Yanagisawa, R.; Ramiere, A.; Volz, S.; Nomura, M. Heat Conduction Tuning by Wave Nature of Phonons. *Sci. Adv.* **2017**, *3* (8).

(15) Yang, B.; Chen, G. Partially Coherent Phonon Heat Conduction in Superlattices. *Phys. Rev. B* **2003**, *67* (19), 195311.

(16) Koh, Y. K.; Cao, Y.; Cahill, D. G.; Jena, D. Heat-Transport Mechanisms in Superlattices. *Adv. Funct. Mater.* **2009**, *19* (4), 610–615.

(17) Luckyanova, M. N.; Garg, J.; Esfarjani, K.; Jandl, A.; Bulsara, M. T.; Schmidt, A. J.; Minnich, A. J.; Chen, S.; Dresselhaus, M. S.; Ren, Z.; et al. Coherent Phonon Heat Conduction in Superlattices. *Science (80-.).* **2012**, *338*, 936–939.

(18) Ravichandran, J.; Yadav, A. K.; Cheaito, R.; Rossen, P. B.; Soukiassian, A.; Suresha, S. J.; Duda, J. C.; Foley, B. M.; Lee, C. H.; Zhu, Y.; et al. Crossover from Incoherent to Coherent Phonon Scattering in Epitaxial Oxide Superlattices. *Nat. Mater.* **2014**, *13* (2), 168–172.

(19) Saha, B.; Koh, Y. R.; Feser, J. P.; Sadasivam, S.; Fisher, T. S.; Shakouri, A.; Sands, T. D. Phonon Wave Effects in the Thermal Transport of Epitaxial TiN/(Al,Sc)N Metal/Semiconductor Superlattices. *J. Appl. Phys.* **2017**, *121* (1), 015109.

(20) Yao, T. Thermal Properties of AlAs/GaAs Superlattices. *Appl. Phys. Lett.* **1987**, *51* (22), 1798–1800.

(21) Chen, G. Size and Interface Effects on Thermal Conductivity of Superlattices and Periodic Thin-Film Structures. *J. Heat Transfer* **1997**, *119* (2), 220–229.

(22) Capinski, W. S.; Maris, H. J.; Ruf, T.; Cardona, M.; Ploog, K.; Katzer, D. S. Thermal-Conductivity Measurements of GaAs/AlAs Superlattices Using a Picosecond Optical Pump-and-Probe Technique. *Phys. Rev. B* **1999**, *59*, 8105.

(23) Hiroi, S.; Nishino, S.; Choi, S.; Seo, O.; Kim, J.; Chen, Y.; Song, C.; Tayal, A.; Sakata, O.; Takeuchi, T. Phonon Scattering at the Interfaces of Epitaxially Grown Fe_2VAl/W and Fe_2VAl/Mo Superlattices. *J. Appl. Phys.* **2019**, *125* (22), 225101.

(24) Choi, S.; Hiroi, S.; Inukai, M.; Nishino, S.; Sobota, R.; Byeon, D.; Mikami, M.; Minamitani, E.; Matsunami, M.; Takeuchi, T. Crossover in Periodic Length Dependence of Thermal Conductivity in 5d Element Substituted Fe_2VAl -Based Superlattices. *Phys. Rev. B* **2020**, *102* (10), 104301.

(25) Harada, S.; Kosaka, N.; Tagawa, M.; Ujihara, T. Ordered Arrangement of Planar Faults with Picoscale Perfection in Titanium Oxide Natural Superlattices. *J. Phys. Chem. C* **2021**, *125* (20), 11175–11181.

(26) Anderson, J. S.; Hyde, B. G. On the Possible Role of Dislocations in Generating Ordered and Disordered Shear Structures. *J. Phys. Chem. Solids* **1967**, *28* (8), 1393–1408.

(27) Harada, S.; Tanaka, K.; Inui, H. Thermoelectric Properties and Crystallographic Shear Structures in Titanium Oxides of the Magnli Phases. *J. Appl. Phys.* **2010**, *108* (8).

(28) Inoue, A.; Iguchi, E. Electrical Properties of Chromia-Doped Rutile (TiO_2). *J. Phys. C Solid State Phys.* **1979**, *12* (23), 5157–5170.

(29) Andersson, S.; Collén, B.; Kuylenstierna, U.; Magnéli, A. Phase Analysis

Studies on the Titanium-Oxygen System. *Acta Chem. Scand.* **1957**, *11*, 1641–1652.

(30) Andersson, S.; Sundholm, A.; Magnéli, A.; Högberg, B.; Kneip, P.; Palmstierna, H. A Homologous Series of Mixed Titanium Chromium Oxides $Ti_{(n-2)}Cr_2O_{(2n-1)}$ Isomorphous with the Series $Ti_{(n)}O_{(2n-1)}$ and $V_{(n)}O_{(2n-1)}$. *Acta Chem. Scand.* **1959**, *13*, 989–997.

(31) Andersson, S.; Templeton, D. H.; Rundqvist, S.; Varde, E.; Westin, G. The Crystal Structure of Ti_5O_9. *Acta Chem. Scand.* **1960**, *14*, 1161–1172.

(32) Bursill, L. A. Crystallographic Shear in Molybdenum Trioxide. *Proc. R. Soc. London. A.* **1969**, *311* (1505), 267–290.

(33) Bursill, L. A.; Hyde, B. G. Crystallographic Shear in the Higher Titanium Oxides: Structure, Texture, Mechanisms and Thermodynamics. *Prog. Solid State Chem.* **1972**, *7*, 177–253.

(34) Philp, D. K.; Bursill, L. A. Phase Analysis Studies of Titanium-Chromium Oxides Derived from Rutile by Crystallographic Shear. *J. Solid State Chem.* **1974**, *10* (4), 357–370.

(35) Bursill, L. A.; Hyde, B. G.; Philp, D. K. New Crystallographic Shear

Families Derived from the Rutile Structure, and the Possibility of Continuous Ordered Solid Solution. *Philos. Mag.* **1971**, *23* (186), 1501–1513.

(36) Gibb, R. M.; Anderson, J. S. The System TiO_2-Cr_2O_3: Electron Microscopy of Solid Solutions and Crystallographic Shear Structures. *J. Solid State Chem.* **1972**, *4* (3), 379–390.

(37) Flörke, O. W.; Lee, C. W. Andersson Phasen, Dichteste Packung Und Wadsley Defekte Im System TiCrO. *J. Solid State Chem.* **1970**, *1* (3–4), 445–453.

(38) Somiya, S.; Hirano, S.; Kamiya, S. Phase Relations of the Cr_2O_3-TiO_2 System. *J. Solid State Chem.* **1978**, *25* (3), 273–284.

(39) Kamiya, S.; Yoshimura, M.; Sōmiya, S. Microstructural Study for a Homologous Series of $Cr_2Ti_{n-2}O_{2n-1}$ with (1-21)r Crystallographic Shear Structure. *Mater. Res. Bull.* **1980**, *15* (9), 1303–1312.

(40) Devi, P. S. Preparation of Fine Particle $Cr_2Ti_2O_7$ Powders by the Citrate Gel Process. *J. Solid State Chem.* **1994**, *110* (2), 345–349.

(41) Thurber, W. R.; Mante, A. J. H. Thermal Conductivity and

Thermoelectric Power of Rutile (TiO_2). *Phys. Rev.* **1965**, *139* (5A), A1655.

(42) Smith, S. J.; Stevens, R.; Liu, S.; Li, G.; Navrotsky, A.; Boerio-Goates, J.; Woodfield, B. F. Heat Capacities and Thermodynamic Functions of TiO_2 Anatase and Rutile: Analysis of Phase Stability. *Am. Mineral.* **2009**, *94* (2–3), 236–243.

(43) Ziman, J. M. *Electrons and Phonons*; Clarendon: Oxford, 1960.

(44) Traylor, J. G.; Smith, H. G.; Nicklow, R. M.; Wilkinson, M. K. Lattice Dynamics of Rutile. *Phys. Rev. B* **1971**, *3* (10), 3457–3472.

Table I. Nominal compositions of the prepared specimens and phases identified by XRD.

Nominal composition (wt% Cr_2O_3)	Phase assemblage
15.0	COSS
20.0	COSS
24.1	$Cr_2Ti_6O_{15}$
27.6	$Cr_2Ti_5O_{13}$ + ($Cr_2Ti_5O_{13}$)

Table II. Estimated values of p' and D_{CS} for the prepared specimens from the analysis of SAED patterns.

Nominal composition (wt% Cr_2O_3)	p'	D_{CS} (nm)
15.0	0.73	1.89
20.0	0.89	1.38
24.1	0.91	1.30
27.6	1	1.14

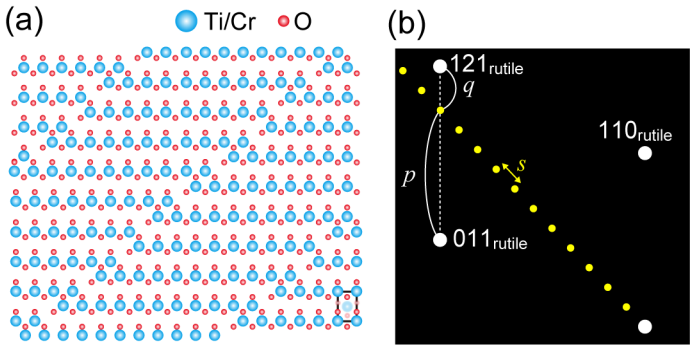

Figure 1. (a) Schematic illustration of atomic arrangement of the COSS phase with $(374)_{rutile}$ CS planes ($p = 3$, $q = 1$, $p' = 0.75$) and $n = 44$ ($Cr_6Ti_{38}O_{85}$), and (b) corresponding SAED patterns along the $[1\text{-}11]_{rutile}$ zone axis. Note that only the superlattice reflection spots from 000_{rutile} are depicted for simplicity.

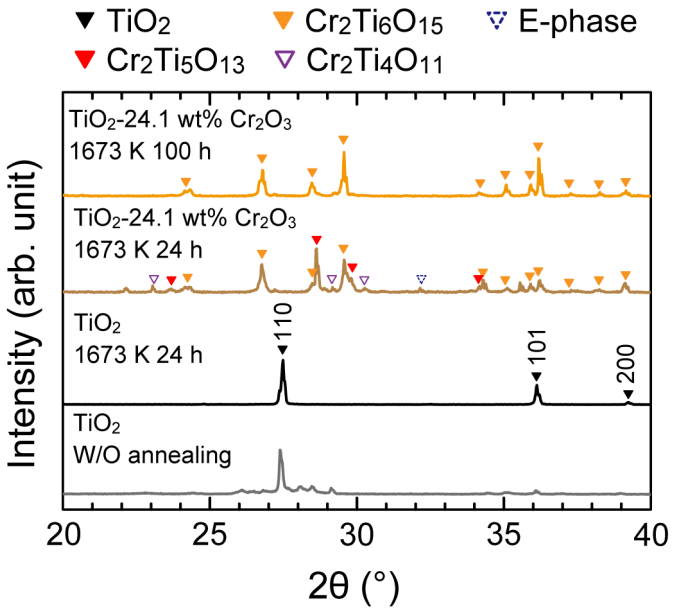

Figure 2. XRD patterns from crystals with nominal compositions of TiO_2 and TiO_2-24.1 wt% Cr_2O_3 prepared by arc-melting under different annealing conditions.

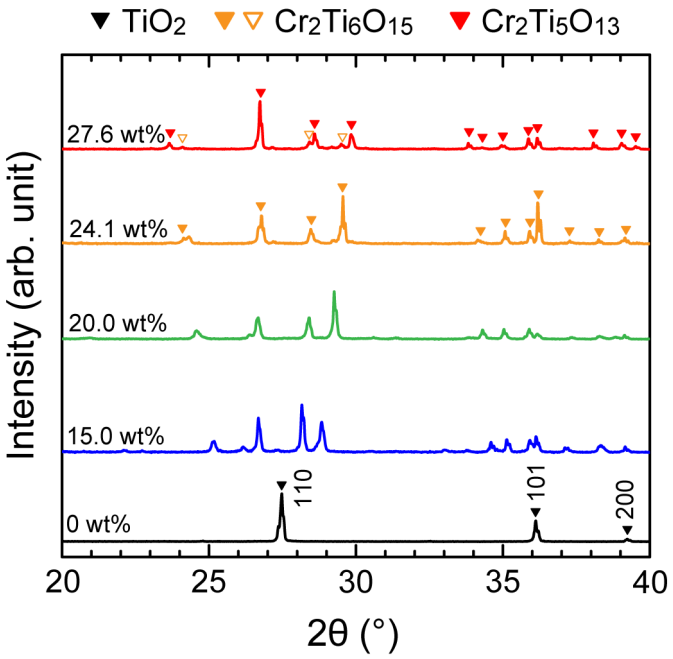

Figure 3. XRD patterns from crystals with nominal compositions of TiO_2-15.0, 20.0, 24.1 and 27.6 wt% Cr_2O_3 after annealing at 1400°C for 100 h.

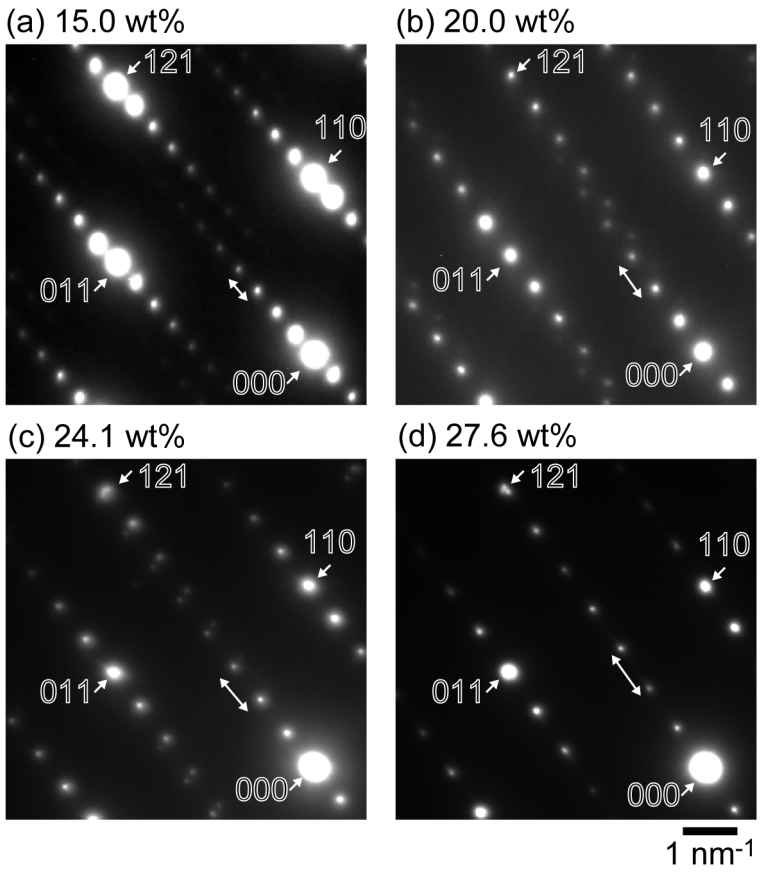

Figure 4. SAED patterns taken from crystals prepared with nominal compositions of (a) 15.0, (b) 20.0, (c) 24.1 and (d) 27.6 wt% Cr_2O_3-TiO_2 along the $[1\text{-}11]_{rutile}$ zone axis. Double arrows indicate the reciprocal spacing and direction of the superlattice spots. All indexes in this figure are of the rutile mother lattice.

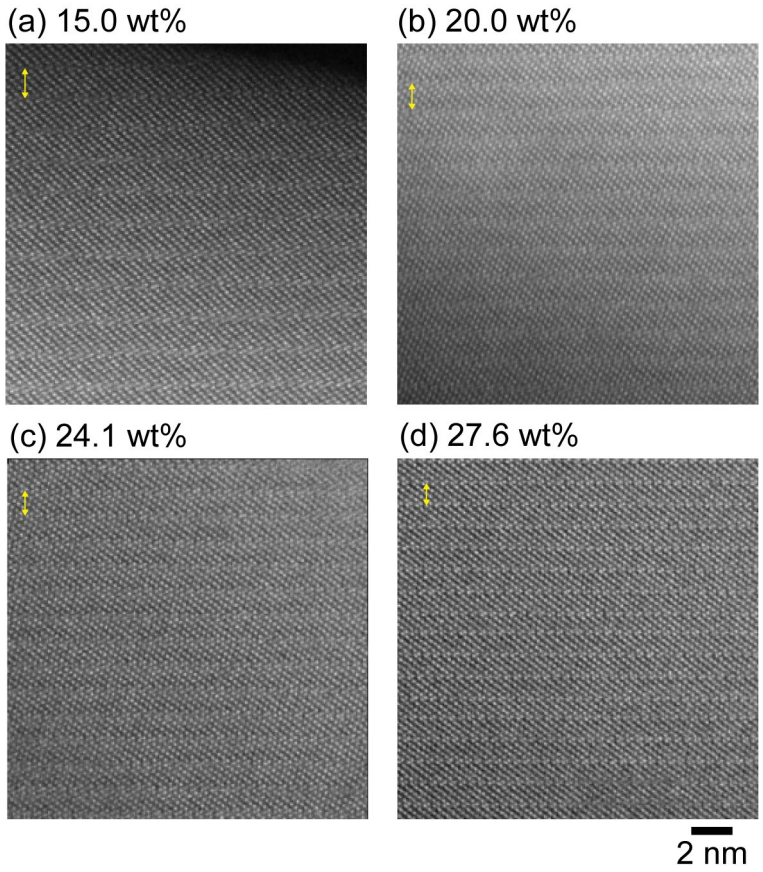

Figure 5. HAADF-STEM images taken from crystals prepared with nominal compositions of (a) 15.0, (b) 20.0, (c) 24.1 and (d) 27.6 wt% Cr_2O_3-TiO_2 along the $[1\text{-}11]_{rutile}$ zone axis. Double arrow signs indicate the typical interspacing of the CS planes.

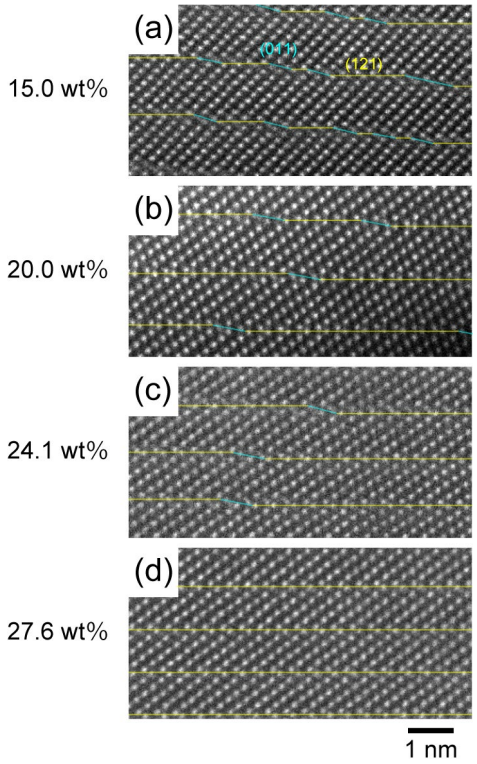

Figure 6. Magnified HAADF-STEM images of crystals prepared with nominal compositions of (a) 15.0, (b) 20.0, (c) 24.1 and (d) 27.6 wt% Cr_2O_3-TiO_2 taken along the $[1\text{-}11]_{rutile}$ zone axis. The positions of CS planes composed of $(121)_{rutile}$ CS planes and $(011)_{rutile}$ APBs are indicated by lines.

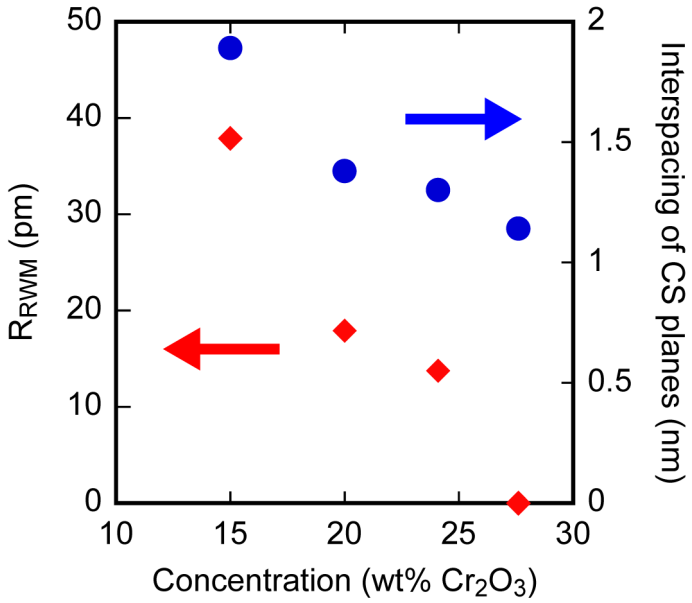

Figure 7. Estimated values of RMS roughness and interspacing of CS planes depending on Cr_2O_3 concentration.